JOURNAL OF GUIDANCE, CONTROL, AND DYNAMICS
Vol. 24, No. 4, July–August 2001

Experimental Evaluation of Flexible Manipulator Trajectory Optimization

Burke Pond* and Inna Sharf†
University of Victoria, Victoria, British Columbia V8W 3P6, Canada

Experimental results showing the effectiveness of trajectory optimization for reducing vibration excitation in point-to-point maneuvers of flexible manipulators are presented. Joint trajectories are found as the solution to a functional (or global) optimization problem. To reduce vibration, the functional is chosen to be the strain energy of the manipulator integrated over the time interval of the motion. A numerical example is presented to help verify the algorithm. A laboratory-based flexible-link manipulator is then described, and a model of its dynamics is obtained by combining analysis with experimental parameter identification. Through the use of the model, the optimal trajectory is generated and compared, both in simulation and experimentally, to a polynomial trajectory and the globally optimal straight-line trajectory. The experiments agree with the simulation in confirming that joint trajectory optimization can significantly reduce the total strain energy incurred during point-to-point motions.

Introduction

ROBOTIC manipulators that are required to have both a long reach and reduced weight typically also possess significant structural flexibility. A prominent example is the space station remote manipulator system to be used in the construction of the space station. A common task for such manipulators, referred to as a point-to-point maneuver, is to move the joints starting from the current configuration and stopping at a given final configuration. To avoid having to compensate for residual vibration of the flexible manipulator, it is also desirable to require that both joint motion and structural vibration are zero at the final configuration. Because point-to-point maneuvers between the given configurations are not unique, a particular maneuver can be selected that is optimal with respect to some objective. In this work we focus on functional, or global, trajectory optimization, in which a cost function is integrated over the time interval of the trajectory.

Optimal slewing of flexible bodies has been considered extensively for space applications.[1] However, such works typically only consider linear, time-invariant dynamics models with a single revolute joint.[2] For example, Thompson et al.[3] construct a nominal, discontinuous bang–bang torque profile smoothed by arctangent functions. The smoothing parameters are chosen first, and then the optimal torque is determined to minimize the slewing time. Although the smoothing gives a near-minimum-time solution, it allows a tradeoff between minimizing maneuver time and minimizing residual vibration.

Another method for eliminating residual vibration in linear, time-invariant systems is referred to as input shaping.[4] A copy of the commanded input (of the same shape but perhaps delayed and scaled) is superimposed on the commanded input to cancel exactly residual vibration. Some robustness properties are derived, and the method is successfully applied to a nonlinear model of the shuttle remote manipulator system undergoing a relatively small-angle, point-to-point maneuver. Banerjee and Singhose[5] consider the application of multimode input shaping for endpoint tracking control of a two-link flexible robot. Their simulation results demonstrate robust performance and significant improvement in repetitive tracking of a fixed trajectory.

For point-to-point maneuvers of a single joint manipulator, the joint path is trivial, and only the speed profile along the path is optimized. Multijoint flexible manipulators permit the optimization of both the joint path and the speed along the path, perhaps given implicitly by the joint accelerations or torques. For redundant manipulators, a tip trajectory is usually specified, and the motion of the redundant degrees of freedom is optimized. For example, Meirovitch and Chen[6] resolved the redundancy of a rigid approximation of a flexible space robot by globally minimizing the norm of the joint rates and then designed a feedback control to reduce the elastic disturbance to the nominal joint trajectory. Note that the trajectory is not determined to minimize vibration. Heuristics may also be used to approximate a globally optimal trajectory.[7,8]

A typical approach to global optimization for general flexible manipulators is to assume some functional form for the solution and to determine the optimal parameters. Mohri et al.[9] calculate the optimal knot points in a B-spline interpolation of the speed profile along a given joint path. Tu and Rastegar,[10] Kim and Rastegar,[11] and Tu and Rastegar[12] have used truncated Fourier series with frequencies chosen not to coincide with the natural frequencies of the system. The optimization objectives were to minimize the energy of the higher harmonics[10,11] or to minimize tip-tracking error.[12] Eisler et al.[13] also did not penalize link vibration, but minimized travel time or tip-tracking error subject to joint torque constraints. Optimization was of 27 joint torque values, which were linearly interpolated for simulation. Zhao and Chen[14] used sinusoids to approximate the tip trajectory of a planar two-link flexible manipulator mounted on a rigid free-floating space station. The two-stage objective was to search for a minimum-time tip trajectory and then obtain a minimum-energy joint trajectory for a particular tip trajectory by a stable inversion approach. The algorithm requires linearization of the zero dynamics, however, and, hence, is suboptimal. To speed optimization, Liu and Kujath[15] generated joint trajectories using profiles with only one unknown parameter, which was then optimized graphically to minimize the norm of the elastic coordinates and rates. Finally, Yao and Cheng[16] expanded the joint angles as fifth-order polynomials plus truncated Fourier series to minimize the global vibration energy. The optimal trajectory generated with a four-term Fourier series was compared in simulation to the (speed) optimized straight-line path in joint space for a planar, two-link flexible manipulator.

Of the works reviewed here, only the last three have considered global trajectory optimization to reduce vibration. The first[14] was suboptimal because the zero dynamics were linearized, the second[15] severely limited the class of comparison trajectories, and the third[16] only presented results for four basis functions without investigating optimality. Furthermore, none of the aforementioned works report experimental results.

In this paper, we determine the optimal joint trajectory among those that achieve the specified point-to-point maneuver. The optimization objective is to minimize the vibration excitation during

Received 15 July 1999; revision received 11 September 2000; accepted for publication 11 September 2000.

*Graduate Student, Department of Mechanical Engineering; currently at Revolve Magnetic Bearings, Inc., Calgary, AB, Canada.

†Associate Professor, Department of Mechanical Engineering, P.O. Box 3055.

the motion, represented by the strain energy integrated over the time interval of the motion. This work presents a general trajectory optimization algorithm applied explicitly to vibration reduction. The methodology is applicable to manipulators with arbitrary mass and stiffness distributions and any joint arrangement. To help verify the algorithm, a numerical example is presented for which the optimal trajectory is nontrivial yet physically justified. Furthermore, the optimal solution calculated numerically is evaluated experimentally. The purpose of the experimental demonstration is to determine the extent to which the generated trajectory improves the actual performance of the manipulator with respect to other trajectories and the given objective functional.

The experimental flexible manipulator, described in the fourth section, is configured so that the globally optimal path in joint space differs in an intuitive way from a straight line. After identifying a suitable model of the manipulator, we compare the globally optimal trajectory with two suboptimal trajectories having straight-line joint paths: one generated by a polynomial and the other by optimizing the speed along the straight-line path. In theory, the globally optimal trajectory minimizes the strain energy integrated over the entire motion. Experimentally, all trajectories are evaluated relative to that same objective. The penultimate section compares the total strain energy incurred by the three trajectories, both in simulation and experimentally. These results allow us to conclude in the final section that the globally optimal trajectory provides significant vibration reduction relative to the other trajectories.

Optimal Motion Planning Problem

Here we develop the motion planning algorithm to be applied to the experimental manipulator in the next section. First, the motion planning problem is formulated as one of functional optimization subject to general flexible manipulator dynamics models. Then, after discussing the numerical implementation of the algorithm, a numerical example is presented to illustrate the algorithm.

Proposed Formulation

This section begins by providing specific details of the functional optimization problem. First, the general structure of the dynamics equations for flexible manipulators is given. This structure allows for some reduction in the complexity of the dynamics constraint for our particular choice of unknown control inputs. The form of the objective functional is then elaborated where, in addition to the particular objective, the strain energy, the boundary conditions and computational tractability also play a role. Finally, to solve the functional optimization problem, an indirect numerical method based on the well-known Pontryagin maximum principle will be applied to the specific problem.

Manipulator Dynamics

For the present purposes, it is sufficient to consider the flexible manipulator dynamics equations in general form; details are given in the cited references.[17] For example, we write the dynamics equations, partitioned into the rigid and elastic part, as

$$\boldsymbol{M}_{rr}(\boldsymbol{q}_r, \boldsymbol{q}_e)\ddot{\boldsymbol{q}}_r + \boldsymbol{M}_{re}(\boldsymbol{q}_r, \boldsymbol{q}_e)\ddot{\boldsymbol{q}}_e + \boldsymbol{h}_r(\boldsymbol{q}_r, \boldsymbol{q}_e, \dot{\boldsymbol{q}}_r, \dot{\boldsymbol{q}}_e) = \boldsymbol{\tau} \quad (1)$$

$$\boldsymbol{M}_{re}^T(\boldsymbol{q}_r, \boldsymbol{q}_e)\ddot{\boldsymbol{q}}_r + \boldsymbol{M}_{ee}(\boldsymbol{q}_r, \boldsymbol{q}_e)\ddot{\boldsymbol{q}}_e + \boldsymbol{K}\boldsymbol{q}_e + \boldsymbol{h}_e(\boldsymbol{q}_r, \boldsymbol{q}_e, \dot{\boldsymbol{q}}_r, \dot{\boldsymbol{q}}_e) = \boldsymbol{0} \quad (2)$$

In these equations, $\boldsymbol{q}_r$ is a column vector of m joint angles, and $\boldsymbol{q}_e$ contains s elastic coordinates obtained from a finite element model of the flexible links. Also, the symmetric manipulator mass matrix $\boldsymbol{M}$ is partitioned as shown, $\boldsymbol{\tau}$ represents the applied joint torques, and $\boldsymbol{K}$ is the manipulator stiffness matrix. (Here the manipulator stiffness matrix is assumed to be constant, according to the common assumption of linear elasticity theory. This assumption is made to simplify some of the calculations, but is not necessary to employ the proposed algorithm.) The $\boldsymbol{h}_r$ and $\boldsymbol{h}_e$ vectors contain the nonlinear inertia terms and gravitational forces.

In typical control formulations, the choice of unknown inputs $\boldsymbol{u} = \boldsymbol{\tau}$ is physically appropriate. For path planning purposes, $\boldsymbol{u}$ can be chosen to be the position coordinates $\boldsymbol{q}$. In the presence of nonintegrable velocity constraints, the velocity $\dot{\boldsymbol{q}}$ of the system could be chosen.[18] However, given the dynamics constraints in our problem [Eq. (2)], we choose $\boldsymbol{u} = \ddot{\boldsymbol{q}}_r$. The advantage of our choice is that the rigid dynamics equations [Eq. (1)] are not necessary for the solution of this problem, but can be used to calculate the torques if desired. Such a calculation is also simpler than the converse one of calculating the accelerations given the torques because the mass matrix $\boldsymbol{M}$ does not need to be inverted. Furthermore, approximations of $\boldsymbol{u}$ by splines or Fourier series can be integrated analytically rather than numerically to determine $\boldsymbol{q}_r$. The dynamics constraint can, therefore, be summarized in state-space form by solving the elastic dynamics [Eq. (2)] for $\ddot{\boldsymbol{q}}_e$ and writing

$$\dot{\boldsymbol{x}} = \boldsymbol{f}(\boldsymbol{x}, \boldsymbol{u}) \quad (3)$$

$$\dot{\boldsymbol{x}} = \begin{pmatrix} \dot{\boldsymbol{q}}_r \\ \dot{\boldsymbol{q}}_e \\ \boldsymbol{u} \\ -\boldsymbol{M}_{ee}^{-1}\left(\boldsymbol{M}_{re}^T\boldsymbol{u} + \boldsymbol{K}\boldsymbol{q}_e + \boldsymbol{h}_e\right) \end{pmatrix} \quad (4)$$

where the n-dimensional state vector is defined to be

$$\boldsymbol{x} := \left(\boldsymbol{q}_r^T, \boldsymbol{q}_e^T, \dot{\boldsymbol{q}}_r^T, \dot{\boldsymbol{q}}_e^T\right)^T \quad (5)$$

for $n = 2(m + s)$ and $\boldsymbol{q}_r \in \mathbb{R}^m$ and $\boldsymbol{q}_e \in \mathbb{R}^s$.

Objective Functional

For a given point-to-point maneuver in joint space, with zero final elastic states, our objective is to find the intervening joint trajectory that minimizes vibration. We choose to represent the total vibration of a trajectory by the manipulator's strain energy

$$V(\boldsymbol{q}_e) := \tfrac{1}{2}\boldsymbol{q}_e^T\boldsymbol{K}\boldsymbol{q}_e \quad (6)$$

integrated over the fixed time interval $[0, T]$ of the trajectory. For now we will also include penalty functions on the final state and control inputs with justification for this approach to follow. Therefore, we choose the following general expression for the cost functional:

$$J[\boldsymbol{u}] = \frac{1}{2}\boldsymbol{x}_e^T\boldsymbol{P}\boldsymbol{x}_e + \frac{1}{2}\int_0^T (\boldsymbol{x}^T\boldsymbol{Q}\boldsymbol{x} + \boldsymbol{u}^T\boldsymbol{R}\boldsymbol{u})\,\mathrm{d}t \quad (7)$$

Here, $\boldsymbol{P}$ and $\boldsymbol{Q} \in \mathbb{R}^{n\times n}$ are constant, positive semidefinite weighting matrices on the final state error $\boldsymbol{x}_e$ and the state $\boldsymbol{x}$, respectively, and $\boldsymbol{R} \in \mathbb{R}^{m\times m}$ is a constant, positive definite weighting matrix on the control inputs. The final state error is

$$\boldsymbol{x}_e := \boldsymbol{x}(T) - \boldsymbol{x}_d \quad (8)$$

where the desired final state $\boldsymbol{x}_d$, prescribed at the final time T, is constant for point-to-point maneuvers. Note that the penalty on the final state error could equivalently be included within the integrand but is written thusly for clarity.

We now specify in detail the weighting matrices $\boldsymbol{P}$, $\boldsymbol{Q}$, and $\boldsymbol{R}$ appropriate to the stated objectives. In accordance with our objective of minimizing the strain energy given by Eq. (6), we choose the block diagonal matrix

$$\boldsymbol{Q} = (1/ET)\,\mathrm{diag}(\boldsymbol{0}, \boldsymbol{K}, \boldsymbol{0}, \boldsymbol{0}) \quad (9)$$

where $\boldsymbol{K}$ is the manipulator's constant stiffness matrix. Each term in J [Eq. (7)] is scaled by a constant characteristic energy value E to make the objective dimensionless. Scaling does not change the optimal solution but facilitates comparison of J values for different manipulators and trajectories. We have chosen $E = ML^2/T^2$ with M and L being the total mass and length of the manipulator, respectively.

Although our primary interest lies in minimizing the strain energy, choosing the input weighting matrix $\boldsymbol{R}$ to be positive definite improves the tractability of the formulation by ensuring that the optimization problem is not singular. A small weighting on the inputs is, therefore, specified by

$$\boldsymbol{R} = \gamma T^3\boldsymbol{I} \quad (10)$$

where $0 < \gamma \ll 1$ is a dimensionless constant and $\boldsymbol{I}$ is the $m \times m$ identity matrix. To penalize errors in the final state, we choose

$$\boldsymbol{P} = \frac{\beta}{E}\begin{bmatrix} \alpha E\boldsymbol{I} & \boldsymbol{0} & \boldsymbol{0} & \boldsymbol{0} \\ \boldsymbol{0} & \boldsymbol{K} & \boldsymbol{0} & \boldsymbol{0} \\ \boldsymbol{0} & \boldsymbol{0} & \boldsymbol{M}_{rr} & \boldsymbol{M}_{re} \\ \boldsymbol{0} & \boldsymbol{0} & \boldsymbol{M}_{re}^T & \boldsymbol{M}_{ee} \end{bmatrix}\Bigg|_{x=x_d} \tag{11}$$

thus weighting the components of the final state error according to an associated energy, either the strain energy, the kinetic energy, or an artificial potential energy of the final joint angle error. The matrix $\boldsymbol{P}$ is made constant by evaluating the constituent block matrices at the desired final state $\boldsymbol{x} = \boldsymbol{x}_d$. The factors α and β are positive, dimensionless constants.

The three terms of the cost J in Eq. (7) represent a penalty on the final state and the integrals of the strain energy and penalty on the inputs, respectively. Thus, β represents the relative weighting assigned to achieving the final state vs minimizing the strain energy en route. Similarly, α weights the artificial potential energy of the final joint angle error relative to the physical energies associated with the other final states. Note that the weight factor γ is chosen to be very small, but not zero, so that the optimization problem is not singular, yet the input costs remain insignificant relative to the strain energy and final state costs.

Optimality

To minimize the objective (7) subject to the nonlinear dynamics (4) we apply the well-known Pontryagin maximum principle (PMP) (see Ref. 19). Introducing the costate vector $\boldsymbol{p}$, we first form the scalar function

$$H(\boldsymbol{x}, \boldsymbol{p}, \boldsymbol{u}) = \tfrac{1}{2}\boldsymbol{x}^T\boldsymbol{Q}\boldsymbol{x} + \tfrac{1}{2}\boldsymbol{u}^T\boldsymbol{R}\boldsymbol{u} + \boldsymbol{p}^T\boldsymbol{f}(\boldsymbol{x}, \boldsymbol{u}) \tag{12}$$

The PMP then implies that a necessary condition for a local minimum is that H be minimized with respect to $\boldsymbol{u}$ at all times. If it is assumed that the set of admissible inputs is not bounded, this condition is equivalent to

$$\frac{\partial H}{\partial \boldsymbol{u}} = \boldsymbol{u}^T\boldsymbol{R} + \boldsymbol{p}^T\frac{\partial \boldsymbol{f}(\boldsymbol{x}, \boldsymbol{u})}{\partial \boldsymbol{u}} = \boldsymbol{0}, \qquad \frac{\partial^2 H}{\partial \boldsymbol{u}^2} = \boldsymbol{R} > 0$$
$$\forall t \in [0, T] \tag{13}$$

Additional necessary conditions are that the state dynamics [Eq. (4)] be satisfied and that the costate evolve according to

$$\dot{\boldsymbol{p}} = -\boldsymbol{Q}\boldsymbol{x} - \left[\frac{\partial \boldsymbol{f}(\boldsymbol{x}, \boldsymbol{u})}{\partial \boldsymbol{x}}\right]^T\boldsymbol{p} \tag{14}$$

subject to the boundary conditions

$$\boldsymbol{x}(0) = \boldsymbol{x}_0, \qquad \boldsymbol{p}(T) = \boldsymbol{P}\boldsymbol{x}_e \tag{15}$$

Rather than solving Eq. (13) for the optimal input $\boldsymbol{u}$ and obtaining a two-point boundary value problem in the state $\boldsymbol{x}$ and costate $\boldsymbol{p}$, the solution algorithm described in the next section will minimize the objective J directly, subject to the state and costate dynamics, and converge to a solution of Eq. (13).

Numerical Solution

For numerical implementation, the infinite dimensional optimization problem is discretized by optimizing the values of the inputs $\boldsymbol{u}_i := \boldsymbol{u}(t_i)$ at N equally spaced knot points t_i, where $i = 1, \ldots, N$, and $t_0 = 0$ and $t_{N+1} = T$. The constraints $\boldsymbol{u}(0) = \boldsymbol{u}(T) = \boldsymbol{0}$ are imposed at the ends of the time interval to enforce continuity. By interpolating between the knot values, $\boldsymbol{u}$ is approximated by the twice continuously differentiable interpolatory cubic spline $\boldsymbol{s}_N(t)$ with clamped end conditions $\dot{\boldsymbol{s}}_N(0) = \dot{\boldsymbol{s}}_N(T) = \boldsymbol{0}$, where $\boldsymbol{s}_N(t_i) = \boldsymbol{u}_i$ (Ref. 20).

An initial estimate for the parameters $\boldsymbol{u}_i$, together with the interpolation, then allows the state dynamics [Eq. (4)] to be integrated forward in time from the given initial state. With both $\boldsymbol{x}$ and $\boldsymbol{u}$ known, the costate dynamics [Eq. (14)] are integrated backwards in time from the given final condition [Eq. (15)]. Finally, the value of the objective J is evaluated.

To improve the convergence rate of the nonlinear optimization, the gradient of the objective with respect to the parameters of $\boldsymbol{u}$ is approximated by

$$\frac{\partial J}{\partial \boldsymbol{u}_i} \approx \Delta t\frac{\partial H}{\partial \boldsymbol{u}_i}, \qquad i = 1, \ldots, N \tag{16}$$

where equality is obtained in the limit as $N \to \infty$. This result agrees with the infinite-dimensional case for which it can be shown that the bounded variation $\delta\boldsymbol{u}$ that minimizes

$$\delta J = \int_0^T \left(\frac{\partial H}{\partial \boldsymbol{u}}\delta\boldsymbol{u}\right) \mathrm{d}t \tag{17}$$

is proportional to $\partial H/\partial \boldsymbol{u}$ (Refs. 21–23). Finally, the gradient of H is determined from the values of the states and costates at each knot point according to Eq. (13), evaluated only at the knot points:

$$\frac{\partial H}{\partial \boldsymbol{u}_i} = \boldsymbol{u}_i^T\boldsymbol{R} + \boldsymbol{p}_i^T\frac{\partial \boldsymbol{f}(\boldsymbol{x}_i, \boldsymbol{u}_i)}{\partial \boldsymbol{u}_i} \tag{18}$$

To implement the numerical optimization, the input vectors $\boldsymbol{u}_i$, $i = 1, \ldots, N$, are assembled into a single vector $\boldsymbol{u}_\Sigma$. With the function value $J(\boldsymbol{u}_\Sigma)$ and its gradient $\partial J/\partial \boldsymbol{u}_\Sigma$ available, determining the optimal value of $\boldsymbol{u}_\Sigma$ becomes a nonlinear multivariable optimization problem. A quasi-Newton numerical optimization scheme, including a line search algorithm, was used to determine the optimal joint acceleration parameters $\boldsymbol{u}_\Sigma$.

Numerical Example

To verify the numerical implementation of the optimization algorithm, this section presents the optimal solution for a point-to-point motion task of a simulated manipulator named REMSPATIAL. The REMSPATIAL manipulator is chosen as a convenient example for which the optimal paths are nontrivial yet physically justifiable. It has two joints (two rigid degrees of freedom) and two links, with the first link rigid and the second link flexible with planar bending only (Fig. 1). A steel sphere at the tip of the flexible aluminum link acts as the payload. Table 1 lists the physical properties of the bodies. The flexible link is modeled by a single beam element giving two elastic coordinates, the deflection and the slope of the tip of the link.

Rotation of the second joint allows any orientation of the bending plane relative to the rotation plane of the first link. In particular, the bending plane of the flexible link can be oriented to decouple the link vibration from motion of the first joint. This configuration thus helps verify motion planning schemes by providing an intuitive solution for trajectories with minimal vibration excitation.

The task is to move the joints from (−90, 0 deg) to (90, 0 deg), rest to rest, in 5 s. The joint accelerations were interpolated using 500 knot points. The weighting factors in the objective are $\alpha = 10^{-1}$, $\beta = 10$, and $\gamma = 10^{-10}$. Figure 2 shows the solution for the optimal joint speed as a function of location along the optimal joint path. As expected, the optimal path first prescribes elbow rotation that orients

Table 1 Physical properties of REMSPATIAL

Body	Dimensions, cm	Mass, kg
Rigid	53 Length	0.8
Elastic	50 × 5 × 0.6	0.4
Sphere	13.4 Diameter	10

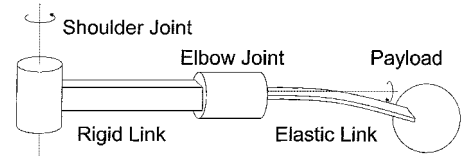

Fig. 1 REMSPATIAL manipulator.

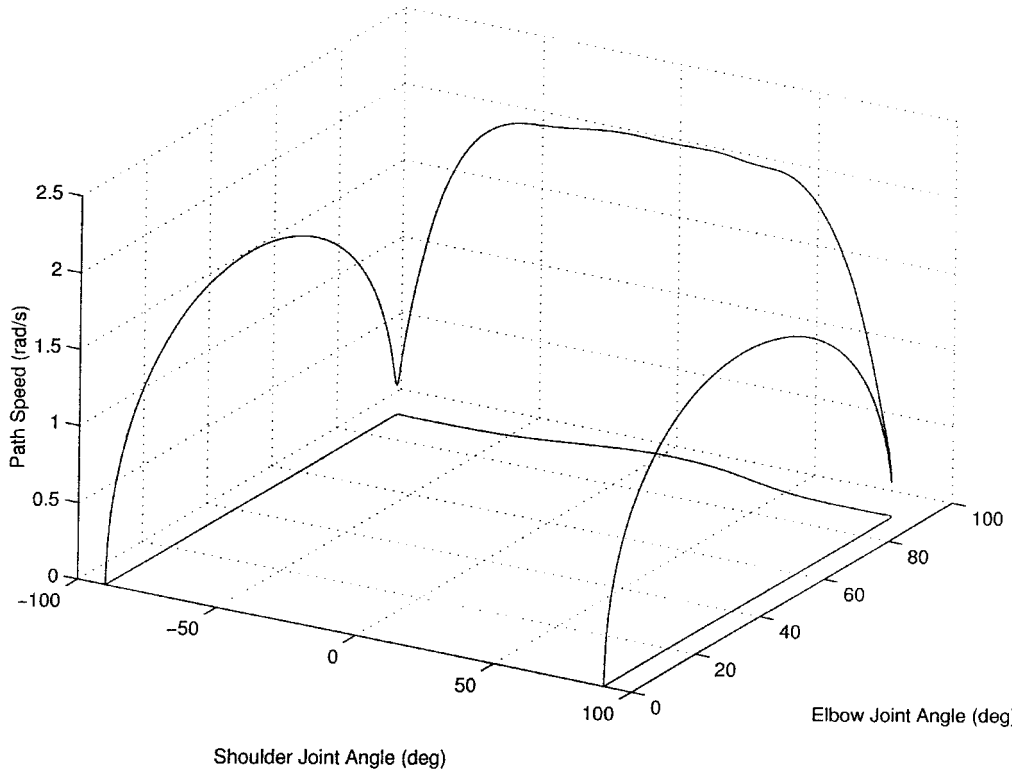

Fig. 2 REMSPATIAL joint speed superimposed on joint path.

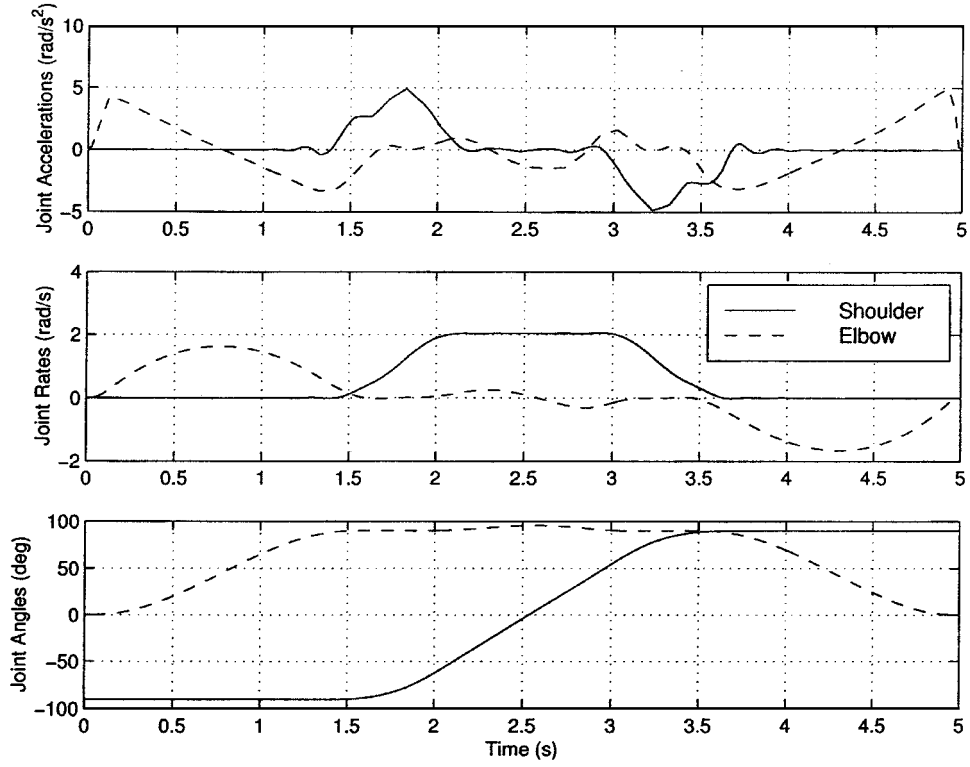

Fig. 3 REMSPATIAL shoulder (——) and elbow (– – –) joint accelerations, rates, and angles.

the flexible link to decouple vibration from shoulder joint rotation. After slewing the shoulder joint, the elbow joint is returned to the desired angle. Because decoupling is complete when the elbow is oriented at ±90 deg, the optimal path incurs zero vibration regardless of the speed along the path. Note that, for the optimal trajectory, only one joint is moving at any particular time, giving zero speed at the sharp corners in the joint path. Simple speed profiles commonly used for point-to-point maneuvers, such as polynomial and trapezoidal, are not well suited to such joint paths.

For verification purposes, the solution for the optimal joint accelerations is shown in Fig. 3, together with the corresponding joint rates and angles. The resulting vibration is represented by the elastic coordinates (Fig. 4) and by the strain energy (Fig. 5), which was the primary component of the optimization objective. Although we expect there to be zero vibration along the optimal path, there is a small amount of strain incurred just before the first corner of the joint path after 1 s. By the 1.5-s mark, it is clear in Fig. 3 that both joints are moving simultaneously. Because the elbow joint is not

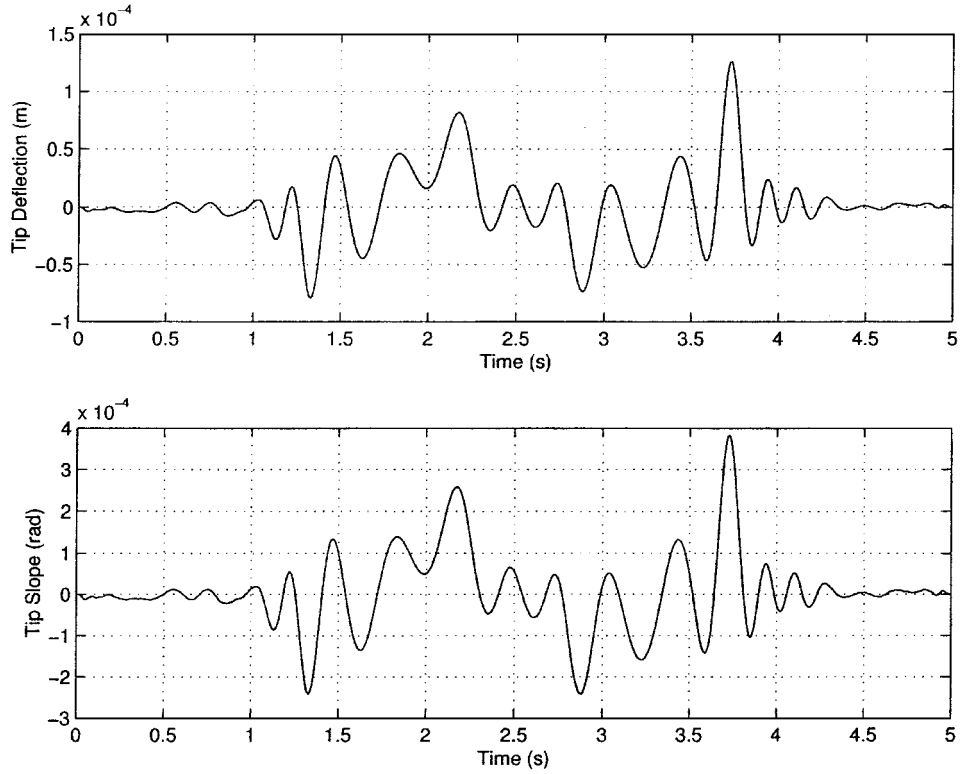

Fig. 4 REMSPATIAL elastic coordinates, flexible link tip deflection, and slope.

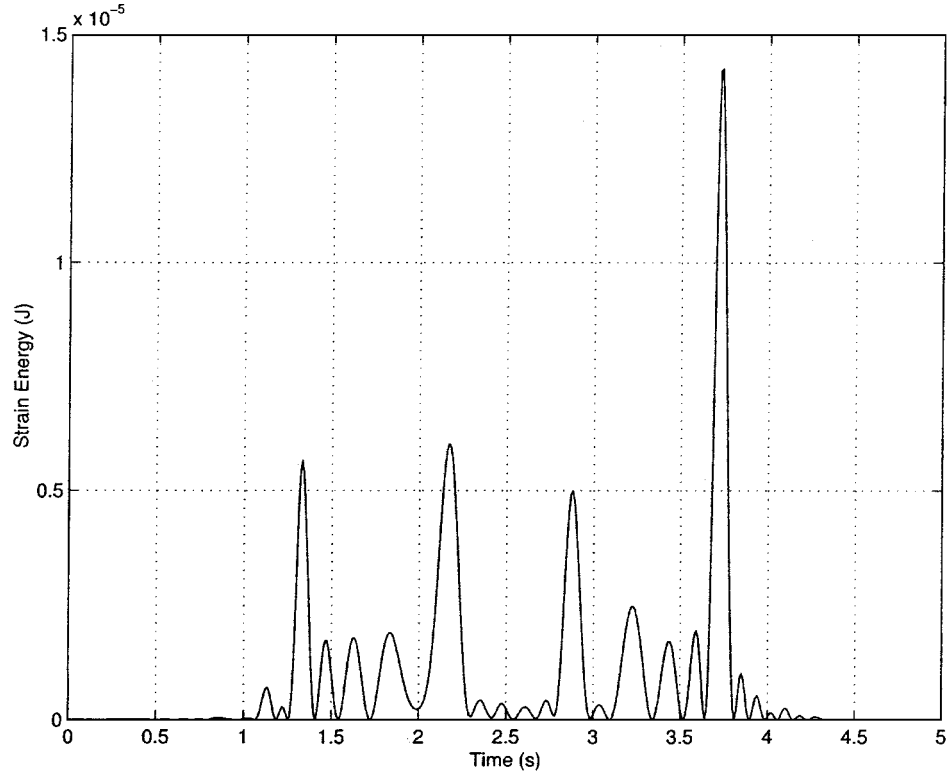

Fig. 5 REMSPATIAL strain energy.

yet at 90 deg, there is a small amount of coupling between shoulder joint acceleration and vibration. Damping of this vibration may also explain the small deviation of the elbow joint from 90 deg at the midpoint of the motion. Comparison of previous results using 50 knot points (not shown) to the results presented here for 500 knot points demonstrated that the significance of both phenomena was greatly reduced with the increase in the number of knot points.

Experimental Flexible Manipulator

This section describes the physical manipulator used for the experiments. The dynamics model of the manipulator employed by the optimization algorithm is based on parameters that were either obtained from an earlier analytical study or identified from experimental vibration testing. The methodology and results of the vibration testing are detailed here, and the joint controller is briefly described.

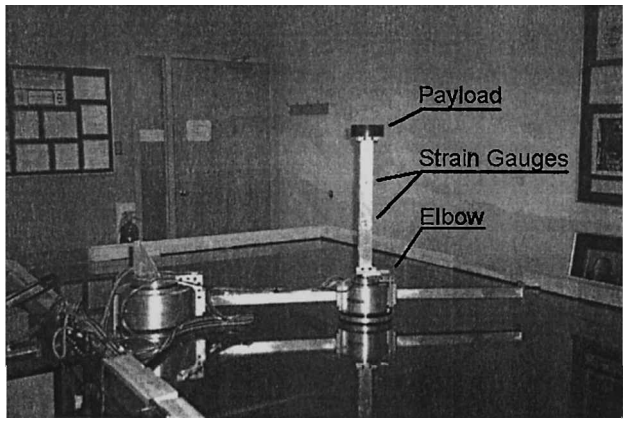

Fig. 6 Experimental flexible manipulator.

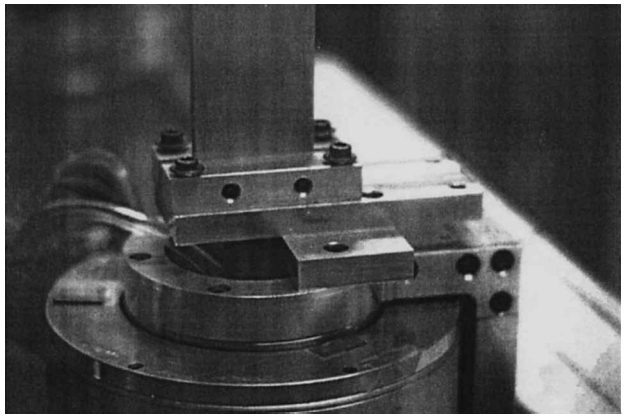

Fig. 7 Attachment of base of flexible link to elbow motor.

Manipulator Construction

The experiments were conducted on a flexible robotics testbed within the Space and Subsea Robotics Laboratory.[24] The flexible manipulator was constructed of two NSK direct-drive motors, the shoulder and the elbow, that were connected by a rigid link and supported by air bearings on a glass table top (Fig. 6). A flexible aluminum link ($6.35 \times 50.8 \times 500$ mm) was mounted vertically along the axis of the elbow motor (Fig. 7) and a payload was attached to the tip of the flexible link. This configuration was chosen so that the orientation of the link's bending plane with respect to the direction of motion of the link's base could be determined by the elbow joint angle. Thus, the coupling of shoulder joint rotation to link vibration could be varied. Note that this particular setup was designed specifically to evaluate the trajectory optimization and not for vibration control. Local strain of the flexible link was sensed by two strain gauges permanently affixed at one-third and two-thirds of the length of the link. A 4.4-kg steel cylinder bolted to the top of the flexible link formed the payload as seen in Fig. 6. Also visible is a horizontal rigid link attached to the output coupler of the elbow motor. This link was included simply to increase the rotational inertia of the payload, thereby improving the trajectory tracking performance of the controller.

Manipulator Model

The properties of the motors were obtained in an earlier study[25] and are listed in Table 2. The properties of the rigid and elastic links are as for the numerical example (Table 1). Because of the vertical orientation of the flexible link, gravity was included in the simulation, although a simple analytical model showed that the first natural frequency would be lowered by only 0.1 Hz. The finite element model of the cantilevered flexible link employed a single beam element. The properties of the payload are included in Table 2.

An additional component of the model was a virtual hinge located at the base of the flexible link. Because the elbow motor was observed to rock within its casing during vibration of the flexible link, the hinge was added to allow an additional degree of freedom between the elbow joint and the flexible link. The hinge was modeled as a rod in torsion with a single elastic degree of freedom and was oriented to rotate in the bending plane of the flexible link. Experimental identification of the radius, rotational inertia, and torsional stiffness of the hinge is described in the next section.

Table 2 Basic physical properties of the experimental manipulator motors and payload

Body	Mass, kg	Dimensions, cm
Shoulder rotor	11.56	Radius: 18
Shoulder output coupler	1.69	——
Elbow input coupler	0.35	——
Elbow case	11.62	——
Elbow rotor	2.95	Radius: 11
Elbow output coupler	0.61	——
Steel cylinder	4.43	Diameter: 12.7; Height: 4.4

Table 3 Parameters of the virtual hinge

Parameter	Value
Radius	0 m
Rotational inertia	$0.05\ \text{kg} \cdot \text{m}^2$
Torsional stiffness	$672\ \text{N} \cdot \text{m}$

Vibration Testing and Parameter Identification

Because the trajectory optimization procedure prescribes trajectories that attempt to dampen vibration at the frequency predicted by the model, and there is no feedback of elastic deformation in these experiments, it is important for the manipulator model to have natural frequencies similar to the experimental manipulator. Otherwise, a large mismatch between actual and model frequencies results in poor damping or even vibration excitation. The parameters of the virtual hinge were, therefore, chosen to attain a satisfactory agreement between the natural frequencies of the model and the experimental manipulator, particularly at the fundamental frequency.

To determine the natural frequencies of the assembled system, vibration of the flexible link was excited in three different ways: plucked, struck, and slapped. For plucking in particular, bending was excited and significant rocking of the elbow motor was also induced. The three spectra of the estimated tip slope (Fig. 8) agree in placing the first natural frequency at 2.5 Hz. In contrast, the numerical model without the hinge predicted a first natural frequency of about 3.75 Hz.

For the purpose of demonstrating the trajectory optimization procedure, the next section shows that matching only the first natural frequency was sufficient to give satisfactory results. To achieve such a match, the radius, rotational inertia, and torsional stiffness of the virtual hinge were adjusted. These three parameters allowed a secondary goal to be achieved, which was to lower the highest natural frequency of the composite model. The highest frequency component has negligible influence on the results, but limits the integration stepsize during numerical simulation.

Table 3 gives the parameters of the virtual hinge obtained by matching the first natural frequency and minimizing the highest frequency. The frequencies were determined from the finite element model of the virtual hinge, link, and payload mass, and the minimization was performed graphically. Clearly, the hinge is a nonphysical addition to the analytical model of the manipulator. The hinge does, however, allow the numerical simulation to match the first natural frequency of the experimental manipulator. For future investigations, the analytical model can be refined by determining the physical nature of the rocking of the elbow motor.

Note that the damping ratio of the flexible link (including rocking of the elbow motor) was determined to be less than 1%. Damping was, therefore, not included in the simulation model.

Joint Controller

Throughout all experiments, a simple proportional–derivative (PD) controller was used for joint trajectory tracking. There were

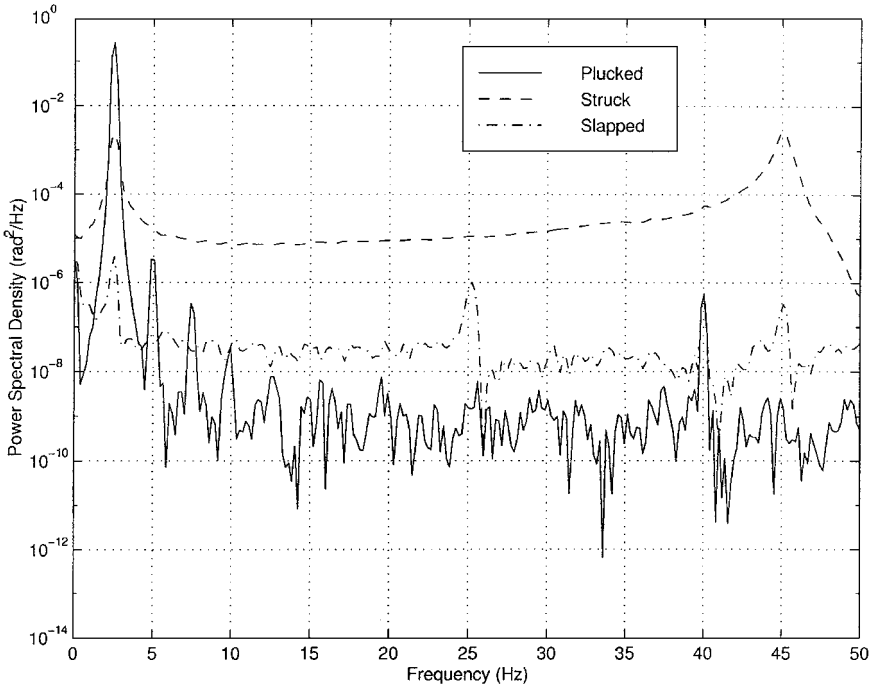

Fig. 8 Power spectral density of flexible link tip slope under different modes of excitation.

Table 4 Independent PD controller feedback gains

Gains\Joint	Shoulder	Elbow
Proportional, N · m/rad	6400	500
Derivative, N · m · s/rad	150	12

100 set points for each of the desired joint angles and desired joint rates linearly interpolated by the controller, which ran at 4000 Hz (Ref. 26). The feedback gains were adjusted independently according to heuristics provided by the motor manufacturer. The resulting gains are listed in Table 4. The performance of the controller will be summarized at the end of the experimental results presented in the next section.

Trajectory Comparison

Having defined a suitable model of the experimental manipulator for input to the global optimization procedure, we can generate point-to-point trajectories for comparison. In this section we present simulation and experimental results showing the performance improvement possible with trajectory optimization.

Task Description

The task considered here is a slew of the shoulder joint while the elbow joint begins and ends the motion with the same orientation. Specifically, the task was to move from (0, 0 deg) to (120, 0 deg) in joint space, rest to rest, in 4 s. Recall that only planar bending of the flexible link was modeled. Elbow joint rotation, thus, varies the orientation of the bending plane with respect to the linear acceleration and velocity of the base of the flexible link. In the 0-deg configuration, the bending plane of the flexible link is perpendicular to the major axis of the rigid link. This task was, therefore, chosen to highlight the vibration decoupling possible by appropriate rotation of the elbow joint, that is, by not following a straight line in joint space.

Trajectory Generation

The motion of the manipulator in joint space can be decomposed into two independent parts: the path of the joints and the speed at which the path is traversed. Other researchers have proposed methods that vary one or the other. For example, the coupling map[7] varies the path but uses a polynomial in time to determine the joint rates and accelerations, whereas other methods vary the speed along the path but do not alter the path. However, functional optimization of the trajectory gives simultaneously the optimal path and speed profile for a given maneuver.

As an illustration of the effects of varying the joint path and speed separately and in combination, we consider the following trajectories for comparison.

Fifth-Order Polynomial

The first trajectory generation method expresses the joint angles as a fifth-order polynomial in time. Besides the specified endpoints, the boundary conditions are zero velocity and acceleration at each end of the trajectory. This common method of trajectory generation always gives straight-line paths in joint space. The speed along the path is also predetermined by the polynomial, and so no optimization takes place. Thus, this particular trajectory demonstrates the case when the trajectory between the endpoints of the maneuvers is specified.

Globally Optimal Straight Line

The second method shows the best that can be achieved without considering different paths in joint space. Only the speed is optimized by constraining the motion to the straight-line path in joint space. Trajectories were generated using the global optimization procedure with cost parameters $\alpha = 10^{-1}$, $\beta = 10$, and $\gamma = 10^{-10}$.

Globally Optimal

Finally, the third method includes the second method but also considers different paths in joint space. The same cost parameters were also used. This is the most general case in which both the joint path and speed are optimized.

In the discussion to follow, we shall refer to each of these three trajectories as polynomial, constrained, and optimal, respectively.

Simulated Results

We now compare the three preceding trajectories as determined through simulation. Figure 9 depicts each of the three paths in the horizontal plane with the path speeds superimposed in the vertical dimension. A physical interpretation of the globally optimal path is as follows. Vibration of the flexible link is excited by linear acceleration of the base of the flexible link, at the elbow joint. (Recall that the model assumes that elbow joint rotation does not excite vibration.) This acceleration lies in the plane of the motors and can be decomposed into two orthogonal components, one tangential to

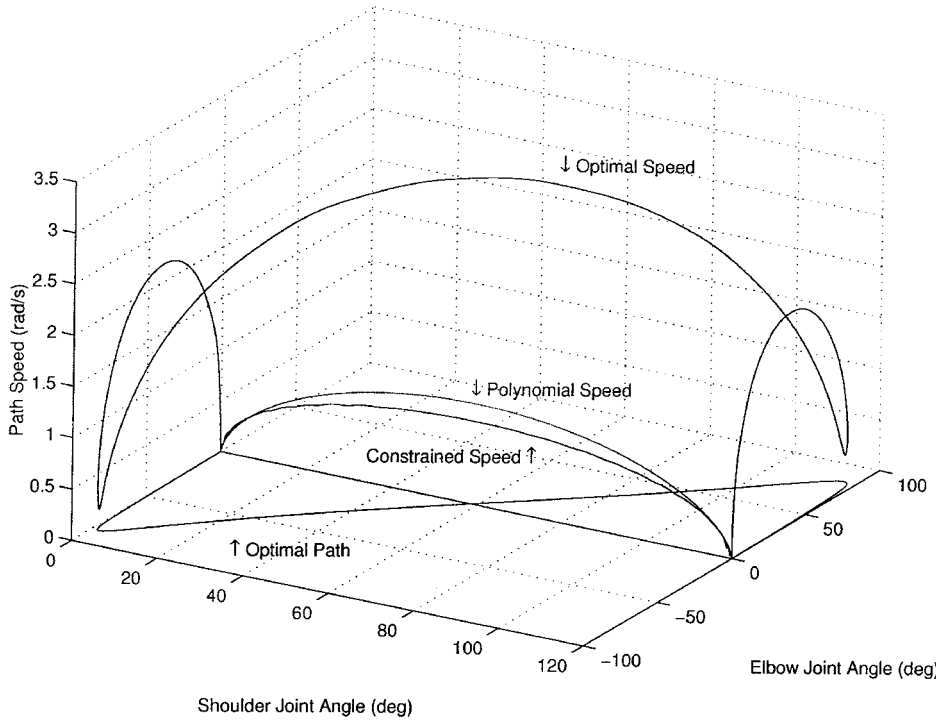

Fig. 9 Joint paths and path speeds from (0, 0 deg) to (120, 0 deg) for three comparison trajectories.

the circular path of the elbow and one radial. When the elbow joint is at 90 deg, the rigid link is in the bending plane of the flexible link. A rotational acceleration of the shoulder joint would result in a tangential acceleration of the base of the flexible link, which is normal to the bending plane. Such normal accelerations excite no vibration. As seen in Fig. 9, the globally optimal path, therefore, begins and ends by orienting the elbow to decouple link vibration from acceleration of the shoulder joint. When the shoulder joint rate is high, but joint acceleration is low, the centripetal (radial) acceleration on the link base becomes more significant than the tangential acceleration, and the decoupled configuration has the elbow at 0 deg.

Although the solution trajectory exhibited some sensitivity to flexible model parameters with respect to the optimal joint speed, motivating the virtual hinge and improved parameter identification, the interpretation of the optimal joint path provided is relatively insensitive to variations in the flexible model parameters. The same optimal path would be expected for any flexible manipulator with the same configuration and a flexible link with different transverse bending stiffnesses.

All of the trajectories compared here satisfy the primary task of point-to-point joint motion, at least within a desired tolerance. Our choice of objective function, however, also reflects our secondary desire to minimize the strain energy created during the motion. The resulting strain energy during the simulated motion is shown in Fig. 10.

To give a more precise comparison of the three trajectories, we tabulate the value of the terms in the objective function [Eq. (7)] for each case. Recall that the three terms in the objective function are the penalty on the final cost, weighted by the $\boldsymbol{P}$ matrix; the integral of the strain energy, weighted by the $\boldsymbol{Q}$ matrix; and the integral of the input cost, weighted by the $\boldsymbol{R}$ matrix. These three terms are labeled final, strain, and inputs, respectively. Table 5 gives these three costs, as well as the total cost, for the three simulated trajectories. Note that, in each case, the cost associated with the strain energy is the greatest, whereas the cost associated with the inputs is the least. Thus, the inclusion of the input cost to make the optimization problem nonsingular has not significantly affected the solution. As expected, the cost associated with the strain energy, as well as the total cost, are least for the optimal trajectory.

Table 5 Objective function costs for simulated trajectories

Task\Cost	Final	Strain	Inputs	Total
Polynomial	1.69e−4	1.39e−3	3.04e−12	1.56e−3
Constrained	2.73e−5	1.00e−3	2.42e−12	1.03e−3
Optimal	4.97e−8	8.21e−6	1.84e−10	8.26e−6

Table 6 Objective function costs for experimental motions

Task\Cost	Final	Strain	Inputs	Total
Polynomial	1.42e−4	3.21e−3	1.29e−9	3.35e−3
Constrained	7.73e−4	2.51e−3	9.18e−10	3.28e−3
Optimal	1.09e−3	6.92e−4	3.65e−8	1.78e−3

Experimental Results

Before presenting the experimental results, it is appropriate to summarize here the performance of the joint controller. Because the actual motion achieved experimentally is not exactly the motion that was prescribed by the simulation results, it is important to characterize the differences, particularly as they relate to vibration excitation.

The actual paths followed experimentally are indistinguishable from the commanded paths at the scale shown earlier in Fig. 9. In fact, the maximum joint angle errors were less than 4 deg. The shoulder joint rate error was less than 5 deg/s although the elbow joint rate error sometimes reached 20 deg/s for the optimal trajectory. All tracking errors were significantly less than these bounds for the straight-line trajectories. Accordingly, the qualitative agreement between simulated and experimental (actual) results is the best for these trajectories.

The actual strain energy for each trajectory was qualitatively the same as predicted, as shown in Fig. 11, although the magnitude was higher than expected. Table 6 shows the costs as measured from experimental data. The value of the integral costs were approximated by the trapezoidal rule. As already alluded, because of the more difficult trajectory tracking requirements of the optimal trajectory, the final cost for the optimal trajectory is higher than for the straight-line trajectories. However, both the strain and total costs remain significantly less than the corresponding costs for the other trajectories.

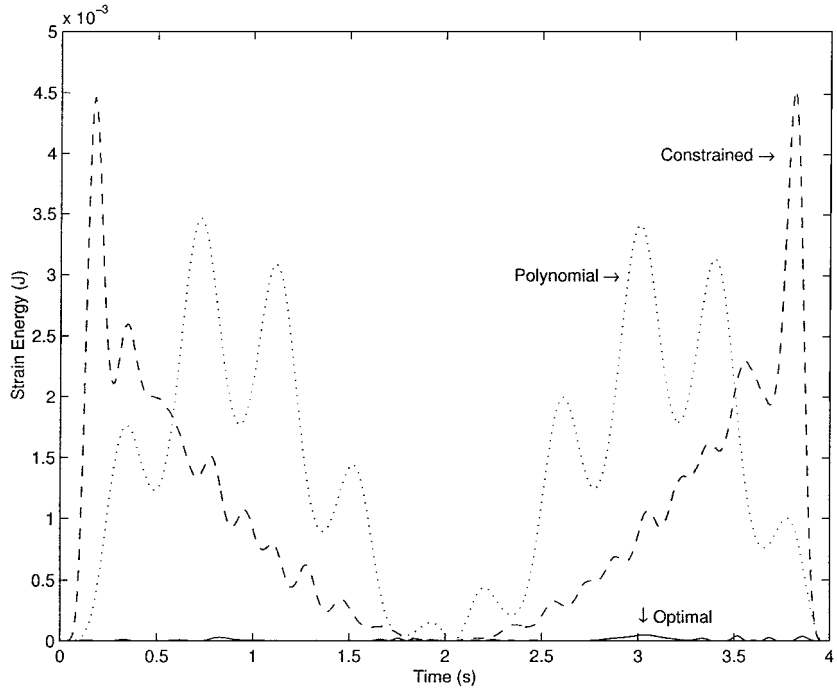

Fig. 10 Simulated strain energies for three comparison trajectories.

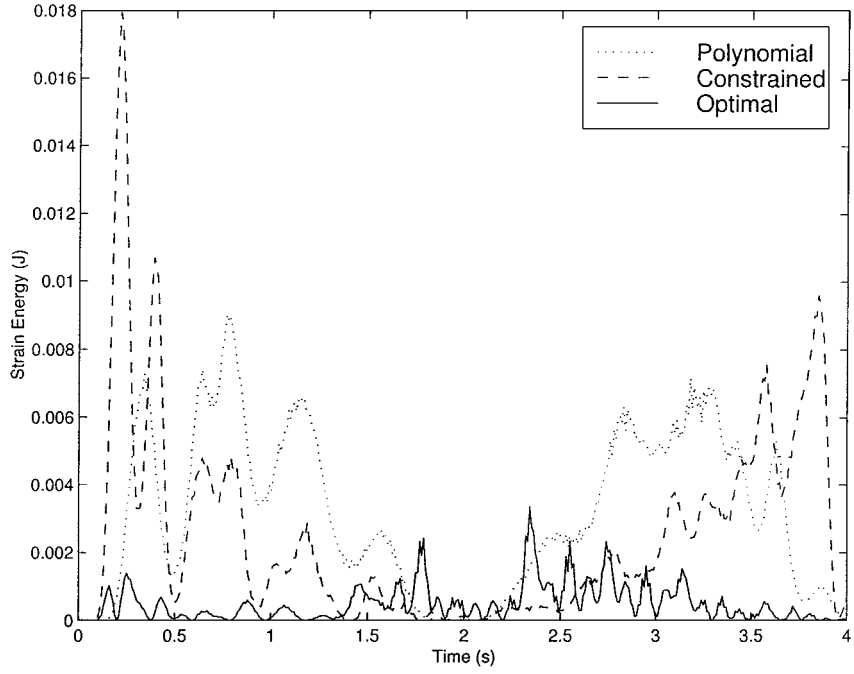

Fig. 11 Experimental strain energies for three comparison trajectories.

Summary and Conclusions

We present a global joint trajectory optimization algorithm to determine the optimal joint trajectory among those that achieve a specified point-to-point maneuver. The optimization objective is to minimize the vibration excitation during the motion, represented by the strain energy integrated over the time interval of the motion. Of the global optimization algorithms proposed in the literature to reduce explicitly vibration in flexible manipulators, the algorithm presented here is more general in that it both allows nonlinear dynamics models and considers a broader class of candidate trajectories. To help verify the algorithm, a numerical simulation example is presented for which the optimal trajectory is nontrivial yet physically justified.

The purpose of this work was to demonstrate experimentally the extent to which a trajectory generated by the global optimization procedure improves the performance of the manipulator with respect to other trajectories and a given objective functional. Specifically, we compared three trajectories for a given point-to-point motion task to evaluate the reduction in strain energy achieved by varying both the joint path and speed along that path. The experimental results presented show that a significant reduction in manipulator vibration can be achieved by employing the global optimization procedure.

Acknowledgments

Many thanks to John Van Vliet for writing the software interface necessary for these experiments and for his many helpful suggestions. This work was supported through the Natural Sciences and Engineering Research Council of Canada Research Grant Program.

References

[1]Hyland, D. C., Junkins, J. L., and Longman, R. W., "Active Control Technology for Large Space Structures," *Journal of Guidance, Control, and Dynamics*, Vol. 16, No. 5, 1993, pp. 801–821.

[2]Suk, J., Kim, Y., and Bang, H., "Experimental Evaluation of the Torque-Shaping Method for Slew Maneuver of Flexible Space Structures," *Journal of Guidance, Control, and Dynamics*, Vol. 21, No. 6, 1998, pp. 817–822.

[3]Thompson, R. C., Junkins, J. L., and Vadali, S. R., "Near-Minimum-Time Open-Loop Slewing of Flexible Vehicles," *Journal of Guidance, Control, and Dynamics*, Vol. 12, No. 1, 1989, pp. 82–88.

[4]Singer, N. C., and Seering, W. P., "Preshaping Command Inputs to Reduce System Vibration," *Journal of Dynamic Systems, Measurement, and Control*, Vol. 112, No. 1, 1990, pp. 76–82.

[5]Banerjee, A. K., and Singhose, W., "Command Shaping in Tracking Control of a Two-Link Flexible Robot," *Journal of Guidance, Control, and Dynamics*, Vol. 21, No. 6, 1998, pp. 1012–1015.

[6]Meirovitch, L., and Chen, Y., "Trajectory and Control Optimization for Flexible Space Robots," *Journal of Guidance, Control, and Dynamics*, Vol. 18, No. 3, 1995, pp. 493–502.

[7]Torres, M. A., and Dubowsky, S., "Path-Planning for Elastically Constrained Space Manipulator Systems," *Proceedings of the 1993 IEEE International Conference on Robotics and Automation*, Vol. 1, IEEE Publications, Piscataway, NJ, 1993, pp. 812–817.

[8]Yoshida, K., Nenchev, D. N., Vichitkulsawat, P., Kobayashi, H., and Uchiyama, M., "Experiments on the PTP Operations of a Flexible Structure Mounted Manipulator System," *Proceedings of the 1996 IEEE/RSJ International Conference on Intelligent Robots and Systems (IROS)*, IEEE Publications, Piscataway, NJ, 1996, pp. 246–251.

[9]Mohri, A., Sarkar, P. K., and Yamamoto, M., "An Efficient Motion Planning of Flexible Manipulator Along Specified Path," *Proceedings of the 1998 IEEE International Conference on Robotics and Automation*, IEEE Publications, Piscataway, NJ, 1998, pp. 1104–1109.

[10]Tu, Q., and Rastegar, J., "Manipulator Trajectory Synthesis for Minimal Vibrational Excitation Due to the Payload," *Transactions of the CSME*, Vol. 17, No. 4A, 1993, pp. 557–566.

[11]Kim, W., and Rastegar, J., "Robot Manipulator Trajectory Synthesis for Minimal Vibrational Excitation," *Proceedings of 1997 ASME DETC*, American Society of Mechanical Engineers, Fairfield, NJ, 1997, pp. 1–10.

[12]Tu, Q., Rastegar, J., and Singh, J. R., "Trajectory Synthesis and Inverse Dynamics Model Formulation and Control of Tip Motion of a High Performance Flexible Positioning System," *Mechanism and Machine Theory*, Vol. 29, No. 7, 1994, pp. 959–968.

[13]Eisler, G. R., Robinett, R. D., Segalman, D. J., and Feddema, J. D., "Approximate Optimal Trajectories for Flexible-Link Manipulator Slewing Using Recursive Quadratic Programming," *Journal of Dynamic Systems, Measurement, and Control*, Vol. 115, No. 13, 1993, pp. 405–410.

[14]Zhao, H., and Chen, D., "Optimal Motion Planning for Flexible Space Robots," *Proceedings of the 1996 IEEE International Conference on Robotics and Automation*, IEEE Publications, Piscataway, NJ, 1996, pp. 393–398.

[15]Liu, K., and Kujath, M. R., "Trajectory Optimization for a Two-Link Flexible Manipulator," *International Journal of Robotics and Automation*, Vol. 11, No. 2, 1996, pp. 56–61.

[16]Yao, C.-M., and Cheng, W.-H., "Joint Space Trajectory Planning for Flexible Manipulators," *Journal of Robotic Systems*, Vol. 12, No. 5, 1995, pp. 287–299.

[17]Hughes, P. C., and Sincarsin, G. B., "Dynamics of an Elastic Multibody Chain: Part B—Global Dynamics," *Dynamics and Stability of Systems*, Vol. 4, Nos. 3 and 4, 1989, pp. 227–244.

[18]Sundar, S., and Shiller, Z., "Optimal Obstacle Avoidance Based on the Hamilton–Jacobi-Bellman Equation," *Proceedings of the 1994 IEEE International Conference on Robotics and Automation*, IEEE Publications, Piscataway, NJ, 1994, pp. 2424–2429.

[19]Athans, M., and Falb, P. L., *Optimal Control*, McGraw–Hill, New York, 1966, p. 288.

[20]Prenter, P. M., *Splines and Variational Methods*, Wiley, New York, 1975, p. 78.

[21]Mufti, I. H., *Computational Methods in Optimal Control Problems*, *Lecture Notes in Operations Research and Mathematical Systems*, Vol. 27, Springer-Verlag, Berlin, 1970, p. 7.

[22]Bryson, Jr., A. E., and Ho, Y.-C., *Applied Optimal Control*, rev. ed., Hemisphere, Washington, DC, 1975, p. 224.

[23]Hasdorff, L., *Gradient Optimization and Nonlinear Control*, Wiley, New York, 1976, p. 115.

[24]Nahon, M., Damaren, C. J., Bergen, A., and Goncalves, J. S., "A Test Facility for Multi-Armed Space-Based Manipulators," *Canadian Aeronautics and Space Journal*, Vol. 41, No. 4, 1995, pp. 150–162.

[25]Stanway, J. S. G., "Validation of a Dynamics Simulation for a Structurally Flexible Manipulator," M.A.Sc. Thesis, Dept. of Mechanical Engineering, Univ. of Victoria, Victoria, BC, Canada, 1996.

[26]Van Vliet, J., and Sharf, I., "Development of a Planar Macro-Micro Manipulator Facility: From Design Through Model Validation," *Canadian Aeronautics and Space Journal*, Vol. 44, No. 1, 1998, pp. 40–50.